JACS
JOURNAL OF THE AMERICAN CHEMICAL SOCIETY
Article
pubs.acs.org/JACS

Phosphorescence versus Thermally Activated Delayed Fluorescence. Controlling Singlet–Triplet Splitting in Brightly Emitting and Sublimable Cu(I) Compounds

Markus J. Leitl,[†] Valentina A. Krylova,[‡] Peter I. Djurovich,[‡] Mark E. Thompson,*[,‡] and Hartmut Yersin*[,†]

[†]Institute for Physical Chemistry, University of Regensburg, 93040 Regensburg, Germany
[‡]Department of Chemistry, University of Southern California, Los Angeles, California 90089, United States

Supporting Information

ABSTRACT: Photophysical properties of two highly emissive three-coordinate Cu(I) complexes, (IPr)Cu(py_2-BMe_2) (**1**) and (Bzl-3,5Me)Cu(py_2-BMe_2) (**2**), with two different N-heterocyclic (NHC) ligands were investigated in detail (IPr = 1,3-bis(2,6-diisopropylphenyl)imidazol-2-ylidene; Bzl-3,5Me = 1,3-bis(3,5-dimethylphenyl)-1*H*-benzo[*d*]imidazol-2-ylidene; py_2-BMe_2 = di(2-pyridyl)dimethylborate). The compounds exhibit remarkably high emission quantum yields of more than 70% in the powder phase. Despite similar chemical structures of both complexes, only compound **1** exhibits thermally activated delayed blue fluorescence (TADF), whereas compound **2** shows a pure, yellow phosphorescence. This behavior is related to the torsion angles between the two ligands. Changing this angle has a huge impact on the energy splitting between the first excited singlet state S_1 and triplet state T_1 and therefore on the TADF properties. In addition, it was found that, in both compounds, spin–orbit coupling (SOC) is particularly effective compared to other Cu(I) complexes. This is reflected in short emission decay times of the triplet states of only 34 μs (**1**) and 21 μs (**2**), respectively, as well as in the zero-field splittings of the triplet states amounting to 4 cm^{-1} (0.5 meV) for **1** and 5 cm^{-1} (0.6 meV) for **2**. Accordingly, at ambient temperature, compound **1** exhibits *two* radiative decay paths which are thermally equilibrated: one via the S_1 state as TADF path (62%) and one via the T_1 state as phosphorescence path (38%). Thus, if this material is applied in an organic light-emitting diode, the generated excitons are harvested mainly in the singlet state, but to a significant portion also in the triplet state. This novel mechanism based on two separate radiative decay paths reduces the overall emission decay time distinctly.

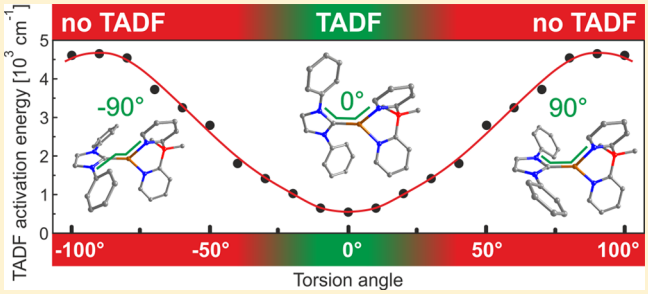

1. INTRODUCTION

In the past years, phosphorescent transition metal compounds have experienced significant research attention as they can be used as highly efficient emitter materials for organic light-emitting diodes (OLEDs).[1,2] Especially, complexes based on third row transition metal ions, such as Ir(III) and Pt(II), are well suited as the heavy metal center can induce significant spin–orbit coupling (SOC). This results in fast intersystem crossings,[3−5] in short emission decay times for the otherwise spin-forbidden transitions from the first excited triplet state to the ground state ($T_1 \rightarrow S_0$),[1,5−15] and to distinct zero-field splittings (ZFS) of the triplet states.[1,5−11] In addition, when applied in an electroluminescent device, these phosphorescent materials show the *triplet harvesting effect* which allows utilizing all excitons, singlets and triplets, for the generation of light.[1,2,10] As a result, emitters that show the triplet harvesting effect can exhibit four times higher exciton to photon conversion efficiencies than conventional purely fluorescent emitters.

However, due to the high cost of iridium and platinum metals, more abundant central metal ions such as Cu(I) are highly attractive and have stepped into the focus of research.[11,16−40] Such compounds might at first sight not seem to be good candidates for use in OLEDs as SOC is significantly less effective in these compounds than in Pt(II) or Ir(III) based complexes due to the smaller SOC constant of copper.[41] As a consequence, phosphorescence decay times of the order of several hundred microseconds can result. This would lead to pronounced saturation effects, if these materials were applied as emitters in OLEDs.[42] On the other hand, the energy separation between the first excited singlet S_1 and triplet T_1 state $\Delta E(S_1 - T_1)$ can be relatively small in Cu(I) compounds due to a small exchange integral resulting from a pronounced metal-to-ligand charge transfer (MLCT) character.[11,16−18,30,34,40,43−45] If this energy separation is small enough, a thermal population of the singlet state from the triplet state becomes efficient at ambient temperature. Thus, a thermally activated delayed fluorescence (TADF) from S_1 to S_0 occurs. As the $S_1 \rightarrow S_0$ transition is spin-allowed, it shows a significantly shorter emission decay time than the correspond-

Received: August 8, 2014
Published: September 26, 2014

   dx.doi.org/10.1021/ja508155x | *J. Am. Chem. Soc.* 2014, 136, 16032−16038

ing triplet state. For this reason, that is, the involvement of the S_1 state emission, the overall decay time of such compounds is drastically reduced and can become as short as only several microseconds at ambient temperature.[11,16−18,30,34,40,43−45] In OLEDs using TADF emitters, the emission largely originates from the singlet state S_1. Therefore, this mechanism has been called *singlet harvesting*[11,16−18,30] in contrast to the *triplet harvesting* effect.

A crucial parameter that determines the effectiveness of the thermally activated delayed fluorescence is the energy separation $\Delta E(S_1 - T_1)$. If it is larger than about 3×10^3 cm^{-1} (0.37 eV), a thermal population of the singlet state S_1 is not effective. Therefore, it is important to understand how $\Delta E(S_1 - T_1)$ can be controlled by properly engineering the chemical structure of an emitter complex. For this, we investigated the two previously published, structurally related Cu(I) complexes (IPr)Cu(py_2-BMe_2) (**1**) and (Bzl-3,5Me)Cu(py_2-BMe_2) (**2**) (IPr = 1,3-bis(2,6-diisopropylphenyl)imidazol-2-ylidene; Bzl-3,5Me = 1,3-bis(3,5-dimethylphenyl)-1H-benzo[d]imidazol-2-ylidene; py_2-BMe_2 = di(2-pyridyl)-dimethylborate).[27] The chemical structures are displayed in Table 1. Interestingly, compound **1** shows a highly effective TADF (with $\Delta E(S_1 - T_1)$ = 740 cm^{-1} (92 meV)), whereas for compound **2** only phosphorescence but no TADF is observed at ambient temperature. In this contribution, we present detailed photophysical characterizations and discuss why despite similar chemical structures the photophysical properties of both compounds differ drastically, especially in regard of the value found for $\Delta E(S_1 - T_1)$.

Table 1. Structures and Emission Properties of the Compounds (IPr)Cu(py_2-BMe_2) (1) and (Bzl-3,5Me)Cu(py_2-BMe_2) (2) as Powders[a]

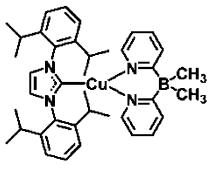

1

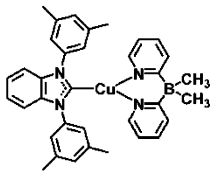

2

	1		2	
Temp. [K]	300	77	300	77
λ_{max} [nm]	475	490	575	585
Φ_{PL} [%]	76	91	73	80
τ [μs]	11	34	18	21
k_r [10^4 s^{-1}]	6.9	2.7	4.1	3.8
k_{nr} [10^4 s^{-1}]	2.2	0.3	1.5	1.0

[a]The decay time is monoexponential in the entire temperature range above ≈25 K. The radiative k_r and nonradiative k_{nr} rates were calculated according to $k_r = \Phi_{PL}\tau^{-1}$ and $k_{nr} = (1 - \Phi_{PL})\tau^{-1}$, respectively.

2. AMBIENT TEMPERATURE PHOSPHORESCENCE VERSUS TADF

Under excitation with UV light, the powders of the studied complexes display intense blue (**1**) and yellow (**2**) luminescence at ambient temperature with short emission decay times of 11 μs (**1**) and 18 μs (**2**) and remarkably high emission quantum yields of 76% (**1**) and 73% (**2**), respectively. In Figure 1, the corresponding emission spectra are displayed.

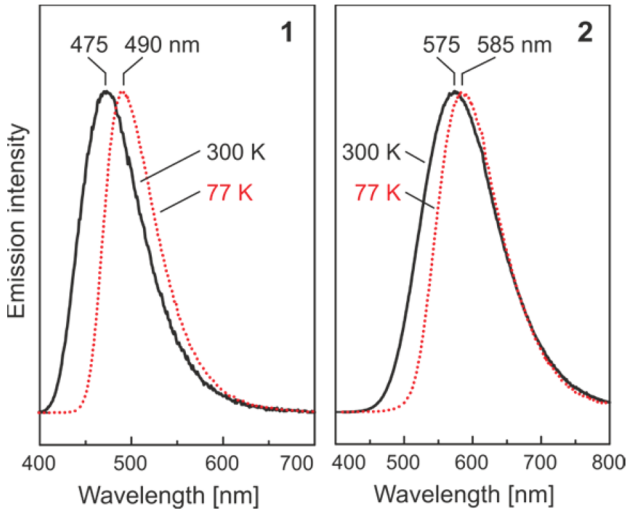

Figure 1. Normalized emission spectra of compound **1** and **2** as powders at ambient temperature and at 77 K. The samples were excited at λ_{exc} = 350 nm.

The spectra are broad and featureless with maxima at 475 nm (**1**) and 575 nm (**2**) at T = 300 K. The shapes of the spectra indicate that the emission originates from a charge transfer transition which, in this case, has significant metal-to-ligand charge transfer (MLCT) character. This assumption is in agreement with literature assignments of other Cu(I) compounds[11,16−20,27−31,43−46] and is further substantiated by results of density functional theory (DFT) and time-dependent density functional theory (TDDFT) calculations presented in ref 27 and below. The emission of **2** is found at significantly lower energy than that of compound **1**. This can be rationalized by the expansion of the π-system of the IPr ligand (compound **2**) which leads to a lower lying LUMO energy than that of the Bzl-3,5Me ligand, whereas HOMOs of both compounds are composed of metal and py_2-BMe_2 orbitals, giving HOMO energies that are nearly unchanged. As a result, the HOMO−LUMO gap and therefore the emission energy are lower for **2** than for **1**.[27]

When cooling from ambient temperature to 77 K, a red-shift of the emission from 475 to 490 nm (≈650 cm^{-1}) is observed for compound **1**. In addition, the emission decay time increases by a factor of about 3 from 11 to 34 μs, whereas the radiative rate $k_r = \Phi_{PL}\tau^{-1}$ decreases by about the same factor from 6.9×10^4 to 2.7×10^4 s^{-1}. The significantly longer emission decay time at 77 K of 34 μs (compared to 11 μs at 300 K) suggests that the emitting state at T = 77 K is the triplet state T_1. Further proof for this assignment is given in subsection 2.2. However, it is remarked that a triplet decay time of 34 μs is extraordinarily short compared to other Cu(I) compounds.[11,16−18,22,25,43] This indicates that SOC is particularly effective in compound **1**. A more detailed discussion of this aspect is given in subsections 2.1 and 2.2. The observed changes of the emission decay time or the radiative rate and the spectral shift of the emission peaks upon temperature change can be explained by the occurrence of a TADF at T = 300 K and are discussed in more detail in subsection 2.2.

In contrast, the emission decay time of compound **2** changes only slightly from 21 to 18 μs when heating from T = 77 K to

dx.doi.org/10.1021/ja508155x | J. Am. Chem. Soc. 2014, 136, 16032−16038

ambient temperature. Almost no change is found for the radiative rate amounting to $k_r(77\ K) = 3.8 \times 10^4\ s^{-1}$ and $k_r(300\ K) = 4.1 \times 10^4\ s^{-1}$, respectively. This indicates that for compound **2** TADF is not effective and that the observed emission even at ambient temperature is phosphorescence stemming from T_1. The slight red-shift of the high energy flank observed on cooling may be explained (especially for this triplet emitter) by freezing out energetically higher lying emissions from an inhomogeneously broadened distribution in the powder sample (compare ref 46) and is therefore *not* a result of the freezing out of the singlet emission. This is in contrast to compound **1** for which the entire spectrum is shifted. (Figure 1) Further support for this rationalization is given by the investigation of the emission spectra in a PMMA (poly(methyl methacrylate)) matrix at 300 and 77 K. In this situation, no such spectral change on temperature variation is observed, besides a slight narrowing on cooling.

2.1. Compound 2: Typical Triplet Emitter. In this subsection, we want to focus on compound **2** by investigating the emission decay time in the temperature range between 1.3 and 300 K (Figure 2) which is particularly instructive.

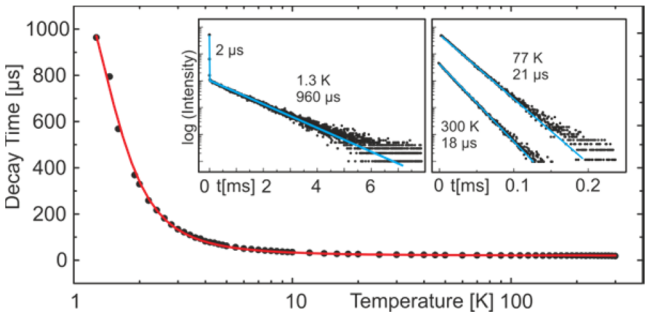

Figure 2. Thermalized emission decay time of compound **2** (powder) versus temperature. The sample was excited at λ_{exc} = 355 nm, and the signal was detected at λ_{det} = 600 nm. The red line represents a fit of the experimental data according to eq 1. Insets: Decay curves at T = 1.3, 77, and 300 K.

From Figure 2, it can be seen that the (thermalized) decay time for compound **2** is almost constant in the temperature range between ≈10 and 300 K and amounts to about 20 μs. Also, the radiative rate is essentially constant (compare Table 1) which allows us to assign the emission as phosphorescence stemming from the T_1 state in the entire temperature range. An emission via the TADF mechanism (compare subsection 2.2) is not occurring in this case. Thus, it can be concluded that the energy splitting $\Delta E(S_1 - T_1)$ between the first excited singlet and triplet state is larger than 3000 cm^{-1} (≈0.4 eV), as for such a large value no significant thermal activation is expected at T = 300 K.

Interestingly, when the temperature is decreased to below ≈10 K a steep increase of the decay time from about 20 μs to 1 ms at T = 1.3 K is observed. A similar behavior is well-known from other transition metal compounds, such as Ir(III) and Pt(II) compounds,[5−8,11,47,48] and can be related to the energy splitting of the triplet state into three substates. This so-called ZFS is a consequence of SOC. Apart from the fast component with a decay time of 2 μs found at T = 1.3 K, the emission decay time at low temperature is governed by a Boltzmann distribution of the three substates I, II, and III. According to the monoexponential decay, these states are in a thermal equilibrium (after several μs). At low temperature, mainly emission from the energetically lowest substates I (and II) is observed. With increasing temperature, the higher lying substate III is thermally populated. Since frequently the radiative rates corresponding to the transitions from the energetically higher lying substates to the S_0 ground state are larger than the rates corresponding to the lowest substate(s), the averaged emission decay time decreases with increasing temperature.[5−8,11,45,47,48] Accordingly, the data given in Figure 2 can be fitted with a modified Boltzmann function (eq 1) in order to determine the ZFS values and the decay time constants of the individual triplet substates (compare refs 7, 45, and 49).

$$\tau(T) = \left[1 + e^{-\frac{\Delta E(II-I)}{k_B T}} + e^{-\frac{\Delta E(III-I)}{k_B T}}\right] \times \left[\tau_I^{-1} + \tau_{II}^{-1} e^{-\frac{\Delta E(II-I)}{k_B T}} + \tau_{III}^{-1} e^{-\frac{\Delta E(III-I)}{k_B T}}\right]^{-1} \quad (1)$$

In this equation, $\tau(T)$ refers to the emission decay time at a given temperature T, τ_I, τ_{II}, and τ_{III} to the individual decay times of triplet substates (I, II, and III), ΔE(III−I) and ΔE(II−I) to the energy splittings between the triplet substates III/I and II/I, respectively, and k_B to the Boltzmann constant.

As a result of the fitting procedure, a value of ΔE(III−I) = ΔE(ZFS) = 5 cm^{-1} (0.6 meV) was found. To the best of our knowledge, such a large ZFS has not been reported before for a Cu(I) complex. However, by this procedure, it could not be determined where substate II is energetically located with respect to substates I and III. If it is assumed that substates I and II are energetically close (ΔE(II−I) ≈ 0 cm^{-1}; compare refs 11, 17, and 18), the emission decay times of the three triplet substates can be obtained. They amount to $\tau_I \approx \tau_{II}$ = 1.5 ms and τ_{III} = 7 μs. The results found for compound **2**, especially the value of ZFS = 5 cm^{-1} and the average emission decay time match well with an empirical ordering scheme that correlates ΔE(ZFS) with the phosphorescence decay time.[1,11] From this perspective, it is not surprising that a ZFS of 5 cm^{-1} is found for a compound with a triplet decay time of about 20 μs.

The short emission decay component of 2 μs at T = 1.3 K becomes shorter and diminishes rapidly with increasing temperature and cannot be observed at temperatures higher than ≈25 K. Such a behavior strongly indicates the occurrence of a relatively slow spin−lattice relaxation (SLR) from the higher lying triplet substate III to the substates I and II according to the *direct* effect of SLR.[5,48] Moreover, in a very rough estimate, one can use the measured value of τ(SLR) = 2 μs to determine the energy separation between the involved states, that is, the value of ΔE(ZFS). With the relation of $\Delta E(ZFS)^3 \sim \tau(SLR)^{-1}$ for the direct process of SLR and the corresponding values known from a number of other organo-transition metal compounds,[5,48] one obtains a value of about 4 cm^{-1} which nicely confirms the splitting values as determined from the fitting procedure as discussed above.

2.2. Compound 1: Thermally Activated Delayed Fluorescence. In Figure 3, the emission decay time of compound **1** is displayed versus temperature. Similar as for compound **2**, two decay components are observed in the temperature range between 1.3 and ≈25 K (not displayed in Figure 3). The short component can again be assigned to SLR processes, whereas the long component corresponds to the thermalized emission of the three triplet substates (compare previous subsection). As for compound **2**, a significant

dx.doi.org/10.1021/ja508155x | J. Am. Chem. Soc. 2014, 136, 16032−16038

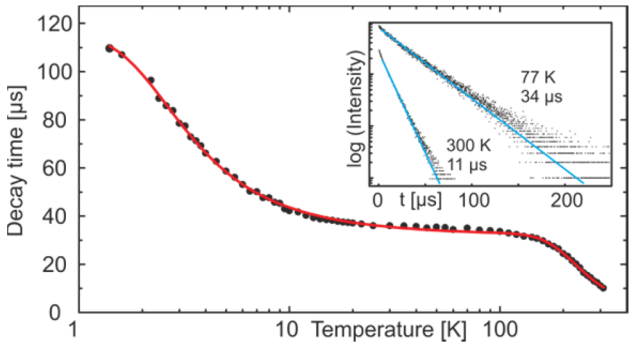

Figure 3. Emission decay time of compound **1** (powder) versus temperature. The sample was excited at λ_{exc} = 378 nm, and the signal was detected at λ_{det} = 490 nm. The red line represents a fit of the experimental data according to eq 2. Inset: Decay curves at T = 77 and 300 K.

reduction of the decay time between T = 1.3 and 10 K from 110 to 40 μs is observed. Again, this can be assigned to the thermal population of higher lying triplet substates from the lowest one(s), leading to an average value of about 34 μs for all three triplet substates between ≈10 and ≈100 K ("plateau").

However, in contrast to the behavior of compound **2**, the emission decay time of compound **1** is not constant up to T = 300 K. It decreases from about 34 to 11 μs at ambient temperature. This effect can be rationalized by the following considerations. At low temperature, only the triplet state T_1 is contributing to the emission. With increasing temperature, a thermal population of the energetically higher lying S_1 state becomes possible. As the S_1 state exhibits a significantly shorter emission decay time than that of the T_1 state, an overall reduction of the emission decay time is observed with increasing temperature. Additionally, a blue-shift of the emission occurs as the S_1 state lies energetically higher than the T_1 state. This emission mechanism corresponds to a thermally activated delayed fluorescence.

The measured data, as displayed in Figure 3, can be fitted with eq 2 which represents an expansion of eq 1 by two additional terms (marked in red), which take the thermal population of the singlet state S_1 into account.

$$\tau(T) = \left[1 + e^{-\frac{\Delta E(II-I)}{k_B T}} + e^{-\frac{\Delta E(III-I)}{k_B T}} + e^{-\frac{\Delta E(S_1-T_1)}{k_B T}}\right] \times \left[\tau_I^{-1} + \tau_{II}^{-1} e^{-\frac{\Delta E(II-I)}{k_B T}} + \tau_{III}^{-1} e^{-\frac{\Delta E(III-I)}{k_B T}} + \tau_{S_1}^{-1} e^{-\frac{\Delta E(S_1-T_1)}{k_B T}}\right]^{-1} \quad (2)$$

From the fitting procedure, the decay times of the three triplet substates of $\tau_I \approx \tau_{II}$ = 116 μs and τ_{III} = 13 μs and a value of ΔE(ZFS) = 4 cm^{-1} (0.5 meV) was found. The latter one is only slightly smaller than found for compound **2**. Similar as for compound **2**, the energy of triplet substate II with respect to substates I and III could not be determined. For the fitting procedure, ΔE(II−I) ≈ 0 cm^{-1} was assumed. The energy splitting between the excited triplet T_1 and singlet state S_1 is determined to $\Delta E(S_1 - T_1)$ = 740 cm^{-1} (90 meV). This value is in good agreement with the blue-shift of the emission spectrum when heating from 77 to 300 K amounting to 650 cm^{-1}. The corresponding emission decay time of the singlet state S_1 is found to be τ(S1) = 160 ns. Such a short decay time emphasizes the singlet nature of this state. It is remarked that in contrast to the delayed fluorescence, a prompt fluorescence is not observed for this compound as intersystem crossing (ISC) from the S_1 to the T_1 state, probably being of the order of 10 ps,[50] is much faster than the prompt $S_1 \rightarrow S_0$ emission.

Interestingly, the increase of the radiative rate and the related decrease of the emission decay time with increasing temperature is for compound **1** significantly less pronounced than that for other Cu(I) complexes. For example, the copper complexes presented in ref 18 show an increase of the radiative rates by the TADF process by a factor of 40−150, whereas compound **1** exhibits only an increase by a factor of 3. An explanation for this behavior can be given when the emission decay path from the triplet state to the singlet ground state is also taken into account. For the compounds in ref 18, the triplet state decay times are long, lying between 250 and 1200 μs, whereas compound **1** exhibits a decay time of only 34 μs. Therefore, a reduction of the decay time by involving the TADF process at higher temperatures is much less effective.

3. CONTROLLING TADF BY LIGAND ORIENTATION

As discussed in section 2, at ambient temperature, compound **1** displays an effective TADF, whereas for compound **2** thermal population of the singlet state is not observed due to the activation energy being greater than 3000 cm^{-1}. Obviously, this effect is connected to differences in the chemical structures of the NHC ligands on the molecules. From Table 2, it can be seen that the compounds differ in two aspects. (i) The π-system of the imidazole ring in compound **1** is expanded by benzannulation in compound **2**. (ii) The isopropyl groups at the 2,6-positions on the pendant phenyl rings of the NHC ligand in **1** are replaced by methyl groups at the 3,5-positions giving compound **2**.

Table 2. Chemical Structures of Compounds 1 and 2 as well as of the Modified Versions 1a and 2a[a]

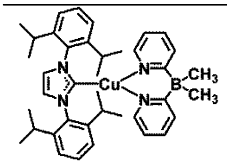	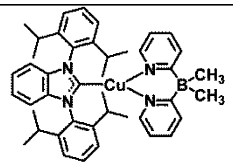
1	**1a**
710 cm^{-1} (740 cm^{-1})	600 cm^{-1}
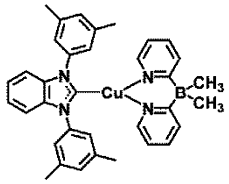	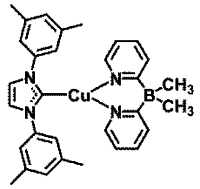
2	**2a**
5800 cm^{-1} (> 3000 cm^{-1})	4200 cm^{-1}

[a]The values for $\Delta E(S_1 - T_1)$ obtained from TDDFT calculations and from experimental investigations (in brackets) are also displayed.

For a better understanding of the effects of these modifications on the energy gap $\Delta E(S_1 - T_1)$ between the first excited singlet and triplet state, we have performed DFT and TDDFT calculations for compounds **1** and **2** as well as for two further model compounds **1a** and **2a** as displayed in Table 2. Compound **1a** represents a modified version of compound **1**

dx.doi.org/10.1021/ja508155x | J. Am. Chem. Soc. 2014, 136, 16032−16038

in which the imidazole ring is π-extended to benzimidazole, but the isopropyl groups on the phenyl rings are retained. Compound **2a** represents a modification of compound **2** where the π-system of the benzimidazole moiety is trimmed to imidazole, but the methyl groups are left unchanged. For all four structures displayed in Table 2, a DFT geometry optimization for the electronic ground state was performed. As starting geometry for compounds **1** and **2**, the crystal structures were used as described and provided in ref 27. The starting geometries for compounds **1a** and **2a** were created by expanding and contracting the π-system, respectively, of the NHC ligand in the structures of compounds **1** and **2**. TDDFT calculations were performed on the structures obtained after geometry optimization.

It was found that compounds **1** and **1a** exhibit very similar (and small) singlet−triplet gaps of 710 and 600 cm^{-1}, respectively. This is in good agreement with the experimental value found for compound **1** amounting to $\Delta E(S_1 - T_1) = 740$ cm^{-1} (compare subsection 2.2). For compounds **2** and **2a**, large values of 5800 and 4200 cm^{-1}, respectively, were found (Table 2). These results indicate that expanding the π-system of the NHC ligand does not have a strong impact on the singlet−triplet splitting. Therefore, these modifications cannot explain the experimentally found differences with values of $\Delta E(S_1 - T_1) = 740$ cm^{-1} for **1** and of $\Delta E(S_1 - T_1) > 3000$ cm^{-1} for **2**.

Interestingly, the insensitivity of the exchange energy to benzannulation of the imidazole ring indicates that the methyl and isopropyl groups present at the IPr and Bzl-3,5Me ligands play an important role for the $\Delta E(S_1 - T_1)$ value and the occurrence of TADF. However, it seems unlikely that these groups impart a direct electronic impact on the singlet−triplet splitting. Instead, the alkyl groups can exert steric control over the orientation of the two ligands toward each other and change the electronic behavior of the compounds in this manner. In support, the X-ray structures (compare ref 27) show that, for compound **1**, the IPr and py_2-BMe_2 ligands are nearly coplanar, whereas for compound **2** the Bzl-3,5Me and py_2-BMe_2 ligands are almost perpendicular to each other (Figure 4).

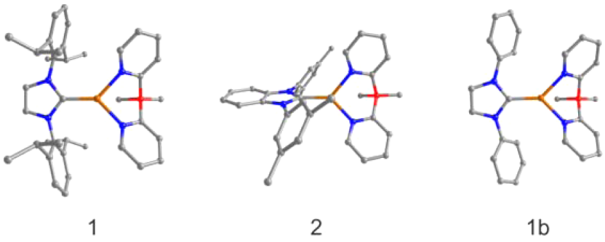

Figure 4. Perspective drawings of the optimized geometries of compounds **1** and **2** as well as of the model compound **1b**. Hydrogen atoms were omitted for clarity.

Thus, we examined how the relative orientations of the ligands toward each other influence the singlet−triplet splitting using a model compound **1b** (Figure 4). In this model compound, the isopropyl groups were removed from the phenyl rings of the NHC ligand. This change allows for variation of the N−C−Cu−N torsion angle (marked green in Figure 6) without encountering steric hindrance from the adjacent py_2-BMe_2 ligand. The N−C−Cu−N torsion angle of **1b** was then fixed at values between 0° and 100° in steps of 10° for a DFT geometry optimization of the singlet ground state. Interestingly, these calculations show that the spatial distribution of the HOMO changes with variation of the torsion angle. In particular, for an angle of 0°, the HOMO is localized on the copper center and py_2-BMe_2 ligand, whereas it is extended onto the imidazole ring when the angle is 90° (compare Figure 5). In

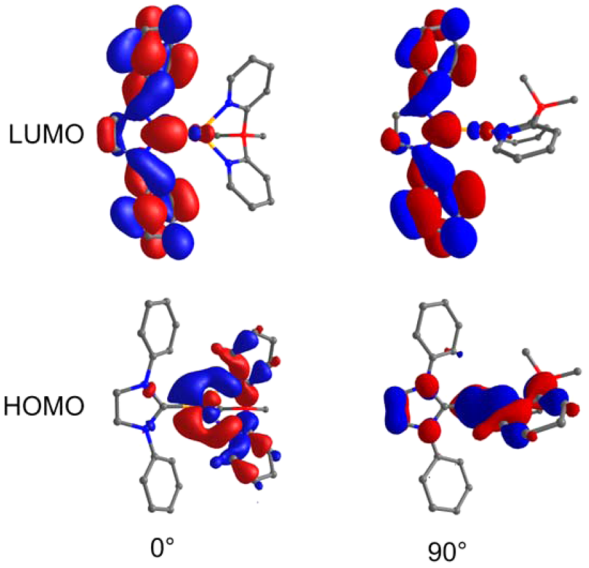

Figure 5. HOMOs and LUMOs of model compound **1b** displayed for a torsion angles of 0° and 90°, respectively.

contrast, the LUMO remains localized on the π*-orbitals of the NHC ligand for all torsion angles. The difference in the HOMO is due to the angular relation between the metal d and imidazole π-orbitals. When the ligands are coplanar, the two sets of orbitals are orthogonal and thus do not electronically couple to each other. However, in the perpendicular orientation, the orbitals have the appropriate symmetry to conjugate and delocalize their electronic distribution onto both ligands. Consequently, overlap between the HOMO and LUMO is small when the torsion angle is 0° (hence a small exchange energy results), whereas a significant overlap exists between the frontier orbitals with a 90° torsion thereby increasing the exchange energy. Since the lowest excited singlet and triplet states are largely comprised from transitions between these frontier orbitals (>94% for the S_1 and >82% for the T_1 state; see Table S1 in the Supporting Information), variation in the degree of overlap will strongly alter the value of $\Delta E(S_1 - T_1)$.

A more accurate estimate of the dependence of the singlet−triplet splitting on the torsion angle can be made when TDDFT calculations are performed on the (torsion constrained) optimized geometries. As compound **1b** exhibits a symmetry element at all rotations (either a mirror plane or a S_2 axis), the values of $\Delta E(S_1 - T_1)$ are identical at positive and negative torsion angles. The data, displayed in Figure 6, show that the singlet−triplet splitting in **1b** is lowest (540 cm^{-1}) when the N−C−Cu−N torsion angle between the two ligands is 0°. This result is in agreement with the experimental data found for compound **1** with a torsion angle of 5° and a singlet−triplet splitting of only 740 cm^{-1}. In contrast, when the torsion angle is 70° (as realized for compound **2**), a splitting of 3700 cm^{-1} is obtained from the calculations. For such a large $\Delta E(S_1 - T_1)$ energy separation, no TADF would occur. These model calculations strongly support the experimental results of a lower

dx.doi.org/10.1021/ja508155x | J. Am. Chem. Soc. 2014, 136, 16032−16038

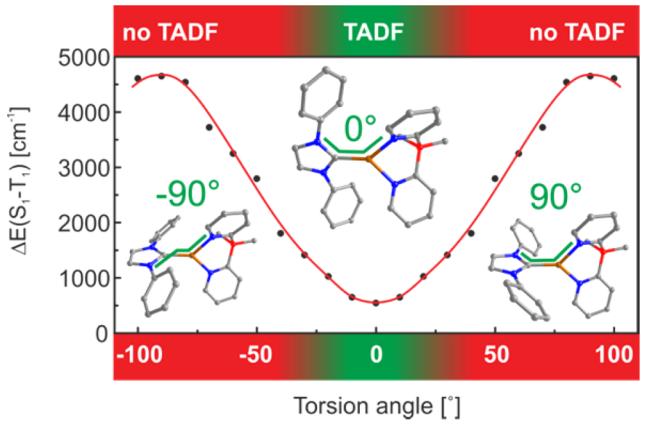

Figure 6. Singlet−triplet splitting $\Delta E(S_1 - T_1)$ in dependence of the torsion angle N−C−Cu−N (marked by the green line) as obtained from DFT and TDDFT calculations on the B3LYP/def2-SVP level of theory.

$\Delta E(S_1 - T_1)$ limit of 3000 cm^{-1} (0.37 eV) as predicted for compound **2**.

4. CONCLUSION

Materials that are applied as emitters in organic light-emitting diodes should be able to utilize all injected excitons for the generation of light. At the moment, these requirements can be met by materials that exhibit the triplet harvesting effect, typically based on high-cost Pt(II) or Ir(III) complexes, or the singlet harvesting effect, typically based on low-cost Cu(I) complexes or specific purely organic materials. Emitters showing the triplet harvesting effect hereby stand out through very effective spin−orbit coupling, whereas emitters exhibiting the singlet harvesting effect excel through a small energy splitting between the first excited triplet and singlet state resulting in a thermally activated delayed fluorescence (TADF).

Both mechanisms lead to an effective reduction of the emission decay time and enable both singlet and triplet excitons to be used for the generation of light in an OLED. One of the compounds presented in this contribution (compound **1**) combines the advantages of both the triplet and the singlet harvesting effect. (i) It exhibits relatively strong spin−orbit coupling which results in a (compared to other Cu(I) compounds known so far) very short triplet emission decay time of only 34 μs. (ii) The energy splitting between the first excited singlet and triplet state amounts to only 740 cm^{-1}. Therefore, the compound exhibits an effective TADF. The contribution of each of the two effects to the emission can be quantified according to the calculations presented in ref 18. It is found that at ambient temperature 38% of the emission intensity stems from the triplet state and 62% from the singlet state. Accordingly, the deactivation via both radiative decay paths induces a greater overall radiative decay rate. Thus, due to the combination of phosphorescence and delayed fluorescence, an effective decay time of τ = 11 μs can be achieved which is shorter than the decay times of the individual processes (τ_{TADF}(300 K) = 16 μs, τ_{Ph} = 34 μs) (Figure 7).

Another important issue that has been revealed in this investigation is the connection between the orientation of the ligands toward each other and the value of the activation energy for a TADF process. The ligand orientation is crucial for the difference between a good OLED emitter with relatively short decay time and an emitter with too long emission decay time

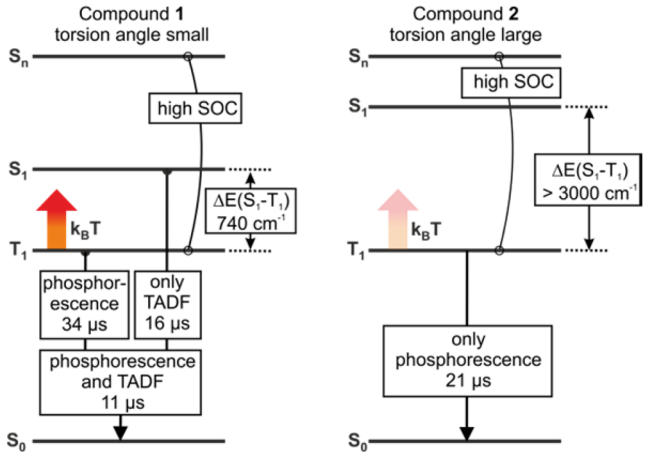

Figure 7. Energy level diagrams of compounds **1** and **2**. At ambient temperature, compound **2** shows only emission from the triplet state, while compound **1** additionally exhibits a TADF. The combination of TADF *and* triplet emission (phosphorescence) results in a distinct reduction of the emission decay time. The triplet states exhibit zero-field splittings of 4 and 5 cm^{-1} for compounds **1** and **2**, respectively. The TADF decay time τ(TADF) at T = 300 K was calculated according to $\tau(\text{phosphorescence and TADF})^{-1} = \tau(\text{phosphorescence})^{-1} + \tau(\text{TADF})^{-1}$. Note that the given phosphorescence decay times are the T = 77 K values.

for good OLED performance. Therefore, the results presented here for the first time give valuable guidelines for the development of new TADF emitter materials.

5. EXPERIMENTAL SECTION

Compounds **1** and **2** were synthesized, purified by vacuum sublimation at 220 °C, and characterized according to the procedures described in ref 27. Absolute measurements of the photoluminescence quantum yields at ambient temperature and at 77 K were performed with a C9920-02 (Hamamatsu Photonics) system. Emission spectra were measured with a Fluorolog 3-22 (Horiba Jobin Yvon) spectrometer which was equipped with a cooled photomultiplier (RCA C7164R). For the measurement of the emission decay times, the same photomultiplier was used in combination with a FAST multichannel scaler PCI card (Comtec). As excitation source for the decay time measurements, a pulsed diode laser (Picobrite PB-375L,) with an excitation wavelength of 378 nm and a pulse width < 100 ps or a pulsed Nd:YAG laser (IB Laser Inc. DiNY pQ 02) with an excitation wavelength of 355 nm and a pulse width < 7 ns was used. For adjusting the temperature, the samples were placed into a helium cryostat (Cryovac Konti Cryostat IT) in which the helium gas flow and heating were controlled. DFT and TDDFT calculations were carried out using NWChem 6.3 on a high performance computing cluster.[51] The calculations were performed on the B3LYP/def2-SVP level of theory,[52,53] which has been shown to give good results for other Cu(I) compounds.[54]

■ ASSOCIATED CONTENT

Supporting Information

HOMO−LUMO coefficients at different torsion angles for compound **1b**. Emission and excitation spectra of compounds **1** and **2** (powder). Absorption spectra of compounds **1** and **2** recorded in dichloromethane. This material is available free of charge via the Internet at http://pubs.acs.org.

■ AUTHOR INFORMATION

Corresponding Authors

hartmut.yersin@ur.de

met@usc.edu

Notes

The authors declare no competing financial interest.

■ ACKNOWLEDGMENTS

We thankfully acknowledge funding by the German Ministry of Education and Research (BMBF). We further appreciate travel expenses provided by the German Academic Exchange Service (DAAD) and the Bavaria California Technology Center (BaCaTec). Furthermore, the authors thank Randy Rückner for support regarding the high performance computation cluster on which the DFT and TDDFT calculations were performed.

■ REFERENCES

(1) Yersin, H., Ed. *Highly Efficient OLEDs with Phosphorescent Materials*; Wiley-VCH: Weinheim, Germany, 2008.
(2) Baldo, M. A.; O'Brien, D. F.; You, Y.; Shoustikov, A.; Sibley, S.; Thompson, M. E.; Forrest, S. R. *Nature* **1998**, *395*, 151−154.
(3) Tang, K.-C.; Liu, K. L.; Chen, I. C. *Chem. Phys. Lett.* **2004**, *386*, 437−441.
(4) Hedley, G. J.; Ruseckas, A.; Samuel, I. D. W. *J. Phys. Chem. A* **2008**, *113*, 2−4.
(5) Yersin, H.; Donges, D. *Top. Curr. Chem.* **2001**, *214*, 81−186.
(6) Rausch, A. F.; Homeier, H. H. H.; Yersin, H. *Top. Organomet. Chem.* **2010**, *29*, 193−235.
(7) Hofbeck, T.; Yersin, H. *Inorg. Chem.* **2010**, *49*, 9290−9299.
(8) Bossi, A.; Rausch, A. F.; Leitl, M. J.; Czerwieniec, R.; Whited, M. T.; Djurovich, P. I.; Yersin, H.; Thompson, M. E. *Inorg. Chem.* **2013**, *52*, 12403−12415.
(9) Rausch, A. F.; Murphy, L.; Williams, J. A. G.; Yersin, H. *Inorg. Chem.* **2011**, *51*, 312−319.
(10) Yersin, H. *Top. Curr. Chem.* **2004**, *241*, 1−26.
(11) Yersin, H.; Rausch, A. F.; Czerwieniec, R.; Hofbeck, T.; Fischer, T. *Coord. Chem. Rev.* **2011**, *255*, 2622−2652.
(12) Cheng, G.; Chow, P.-K.; Kui, S. C. F.; Kwok, C.-C.; Che, C.-M. *Adv. Mater.* **2013**, *25*, 6765−6770.
(13) Sajoto, T.; Djurovich, P. I.; Tamayo, A. B.; Oxgaard, J.; Goddard, W. A.; Thompson, M. E. *J. Am. Chem. Soc.* **2009**, *131*, 9813−9822.
(14) Fernandez-Hernandez, J. M.; Beltran, J. I.; Lemaur, V.; Galvez-Lopez, M. D.; Chien, C. H.; Polo, F.; Orselli, E.; Fröhlich, R.; Cornil, J.; De Cola, L. *Inorg. Chem.* **2013**, *52*, 1812−1824.
(15) Tarran, W. A.; Freeman, G. R.; Murphy, L.; Benham, A. M.; Kataky, R.; Williams, J. A. G. *Inorg. Chem.* **2014**, *53*, 5738−49.
(16) Czerwieniec, R.; Kowalski, K.; Yersin, H. *Dalton T.* **2013**, *42*, 9826−9830.
(17) Czerwieniec, R.; Yu, J.; Yersin, H. *Inorg. Chem.* **2011**, *50*, 8293−8301.
(18) Leitl, M. J.; Küchle, F. R.; Mayer, H. A.; Wesemann, L.; Yersin, H. *J. Phys. Chem. A* **2013**, *117*, 11823−11836.
(19) Krylova, V. A.; Djurovich, P. I.; Aronson, J. W.; Haiges, R.; Whited, M. T.; Thompson, M. E. *Organometallics* **2012**, *31*, 7983−7993.
(20) Krylova, V. A.; Djurovich, P. I.; Whited, M. T.; Thompson, M. E. *Chem. Commun.* **2010**, *46*, 6696−6698.
(21) Tsuge, K. *Chem. Lett.* **2013**, *42*, 204−208.
(22) Osawa, M. *Chem. Commun.* **2014**, *50*, 1801−1803.
(23) Kobayashi, A.; Komatsu, K.; Ohara, H.; Kamada, W.; Chishina, Y.; Tsuge, K.; Chang, H. C.; Kato, M. *Inorg. Chem.* **2013**, *52*, 13188−13198.
(24) Kaeser, A.; Mohankumar, M.; Mohanraj, J.; Monti, F.; Holler, M.; Cid, J. J.; Moudam, O.; Nierengarten, I.; Karmazin-Brelot, L.; Duhayon, C.; Delavaux-Nicot, B.; Armaroli, N.; Nierengarten, J. F. *Inorg. Chem.* **2013**, *52*, 12140−12151.
(25) Zhang, Q.; Komino, T.; Huang, S.; Matsunami, S.; Goushi, K.; Adachi, C. *Adv. Funct. Mater.* **2012**, *22*, 2327−2336.
(26) Wada, A.; Zhang, Q.; Yasuda, T.; Takasu, I.; Enomoto, S.; Adachi, C. *Chem. Commun.* **2012**, *48*, 5340−5342.
(27) Krylova, V. A.; Djurovich, P. I.; Conley, B. L.; Haiges, R.; Whited, M. T.; Williams, T. J.; Thompson, M. E. *Chem. Commun.* **2014**, *50*, 7176−7179.
(28) Wallesch, M.; Volz, D.; Zink, D. M.; Schepers, U.; Nieger, M.; Baumann, T.; Bräse, S. *Chem.—Eur. J.* **2014**, *20*, 6578−6590.
(29) Zink, D. M.; Volz, D.; Baumann, T.; Mydlak, M.; Flügge, H.; Friedrichs, J.; Nieger, M.; Bräse, S. *Chem. Mater.* **2013**, *25*, 4471−4486.
(30) Zink, D. M.; Bächle, M.; Baumann, T.; Nieger, M.; Kuhn, M.; Wang, C.; Klopper, W.; Monkowius, U.; Hofbeck, T.; Yersin, H.; Bräse, S. *Inorg. Chem.* **2013**, *52*, 2292−2305.
(31) Volz, D.; Nieger, M.; Friedrichs, J.; Baumann, T.; Bräse, S. *Langmuir* **2013**, *29*, 3034−3044.
(32) Cunningham, C. T.; Moore, J. J.; Cunningham, K. L. H.; Fanwick, P. E.; McMillin, D. R. *Inorg. Chem.* **2000**, *39*, 3638−3644.
(33) Cid, J. J.; Mohanraj, J.; Mohankumar, M.; Holler, M.; Monti, F.; Accorsi, G.; Karmazin-Brelot, L.; Nierengarten, I.; Malicka, J. M.; Cocchi, M.; Delavaux-Nicot, B.; Armaroli, N.; Nierengarten, J. F. *Polyhedron* **2014**, *82*, 158−172.
(34) Linfoot, C. L.; Leitl, M. J.; Richardson, P.; Rausch, A. F.; Chepelin, O.; White, F. J.; Yersin, H.; Robertson, N. *Inorg. Chem.* **2014**, *53*, 10854−10861.
(35) Igawa, S.; Hashimoto, M.; Kawata, I.; Yashima, M.; Hoshino, M.; Osawa, M. *J. Mater. Chem. C* **2013**, *1*, 542−551.
(36) Lotito, K. J.; Peters, J. C. *Chem. Commun.* **2010**, *46*, 3690−3692.
(37) Vitale, M.; Ford, P. C. *Coord. Chem. Rev.* **2001**, *219−221*, 3−16.
(38) Zigler, D. F.; Tordin, E.; Wu, G.; Iretskii, A.; Cariati, E.; Ford, P. C. *Inorg. Chim. Acta* **2011**, *374*, 261−268.
(39) Kutal, C. *Coord. Chem. Rev.* **1990**, *99*, 213−252.
(40) Yersin, H.; Leitl, M. J.; Czerwieniec, R., In *Organic Light Emitting Materials and Devices XVIII*; So, F., Adachi, C., Eds.; Proceedings of SPIE; SPIE: Bellingham, WA, 2014; Vol 9183, 91830N-1 - 91830N-11.
(41) Murov, S. L.; Hug, G. L.; Carmichael, I. *Handbook of Photochemistry*, 2nd ed.; Marcel Dekker: New York, 1993; pp 339−341.
(42) Murawski, C.; Leo, K.; Gather, M. C. *Adv. Mater.* **2013**, *25*, 6801−6827.
(43) Deaton, J. C.; Switalski, S. C.; Kondakov, D. Y.; Young, R. H.; Pawlik, T. D.; Giesen, D. J.; Harkins, S. B.; Miller, A. J. M.; Mickenberg, S. F.; Peters, J. C. *J. Am. Chem. Soc.* **2010**, *132*, 9499−9508.
(44) Palmer, C. E. A.; McMillin, D. R. *Inorg. Chem.* **1987**, *26*, 3837−3840.
(45) Blasse, G.; McMillin, D. R. *Chem. Phys. Lett.* **1980**, *70*, 1−3.
(46) Coppens, P.; Sokolow, J.; Trzop, E.; Makal, A.; Chen, Y. *J. Phys. Chem. Lett.* **2013**, *4*, 579−582.
(47) Rausch, A. F.; Thompson, M. E.; Yersin, H. *Chem. Phys. Lett.* **2009**, *468*, 46−51.
(48) Yersin, H.; Strasser, J. *Coord. Chem. Rev.* **2000**, *208*, 331−364.
(49) Azumi, T.; O'Donnell, C. M.; McGlynn, S. P. *J. Chem. Phys.* **1966**, *45*, 2735−2742.
(50) Iwamura, M.; Watanabe, H.; Ishii, K.; Takeuchi, S.; Tahara, T. *J. Am. Chem. Soc.* **2011**, *133*, 7728−7736.
(51) Valiev, M.; Bylaska, E. J.; Govind, N.; Kowalski, K.; Straatsma, T. P.; Van Dam, H. J. J.; Wang, D.; Nieplocha, J.; Apra, E.; Windus, T. L.; de Jong, W. A. *Comput. Phys. Commun.* **2010**, *181*, 1477−1489.
(52) Becke, A. D. *J. Chem. Phys.* **1993**, *98*, 5648.
(53) Weigend, F.; Ahlrichs, R. *Phys. Chem. Chem. Phys.* **2005**, *7*, 3297−3305.
(54) Jesser, A.; Rohrmüller, M.; Schmidt, W. G.; Herres-Pawlis, S. *J. Comput. Chem.* **2014**, *35*, 1−17.